Eur. Phys. J. E **24**, 229–241 (2007)
DOI 10.1140/epje/i2007-10230-4

THE EUROPEAN PHYSICAL JOURNAL E

Compressing a rigid filament: Buckling and cyclization

N.-K. Lee[1,a], A. Johner[2], and S.-C. Hong[3]

[1] Institute of Fundamental Physics, Department of Physics, Sejong University, Seoul 143-743, South Korea
[2] Institut Charles Sadron, 67083 Strasbourg Cedex, France
[3] Department of Physics, Korea University, Seoul 136-713, Korea

Received 8 July 2007 and Received in final form 28 September 2007
Published online: 9 November 2007 –

Abstract. We study elastic properties of rigid filaments modeled as stiff chains shorter than their persistence length. By rigid filaments we mean that fluctuations around the optimal filament shape are weak and that low-order expansions (quadratic or quartic) in the deviation from the optimal shape are sufficient to describe them. Our main interest lies in the profiles of force *vs.* projected filament length, closure probability and weakly buckled states. Results may be relevant to experiments on self-assembled biological (microtubules, actin filaments) and synthetic (organo-gelators) filaments, carbon nanotubes and polymers grafted with strongly repelling side chains, some of which are discussed here.

PACS. 82.37.Rs Single molecule manipulation of proteins and other biological molecules – 87.16.Ka Filaments, microtubules, their networks, and supramolecular assemblies – 87.15.La Mechanical properties

1 Introduction

Stiff molecules play an important role in both natural and synthetic systems [1–3]. In particular, molecules such as CNT (Carbon NanoTube) and DNA are extremely useful from the technological point of view. Other kinds of rigid filament are provided by self-assembling tubulin or actin and synthetic organo-gelators or polypeptides. Over the last decade, the advances in nanotechnology allow the manipulation of a single molecule [4–7]. Using optical/magnetic tweezers, numerous experiments on pulling various molecules have been performed. A large number of theoretical studies [8–11] predict the force-extension relation of stiff molecules during pulling which is a central quantity for many DNA or RNA experiments [4–7,12]. However, relatively few studies have been devoted to compressed filaments [13–15]. Compressing only makes sense for rigid filaments that do not coil under thermal fluctuations: microtubules (MT), CNT, actin filaments, some synthetic self-assembled filaments, short DNA fragments and short helical or conjugated polymer fragments are a few examples. The common buckling instability of macroscopic rigid rods also occurs to stiff filaments. Such transitions can be used to design nanoscale switches based on conducting CNT. In a celebrated seminal two-dimensional (2-d) experiment, Dogterom *et al.* estimated the pushing force necessary to prohibit growth of microtubule filament [16,17], so-called stall force, from the (stable) buckled shape of a microtubule filament compressed between a centrosome which it originates from and a (cell) wall [18]. Elasticity of filaments also governs the mechanical response of systems [19] involving many filaments like networks built from self-assembling biomolecules (actin) [20], entangled solutions [21] or bundles [13] and assemblies of bundles [22]. Buckling of a rigid filament and its strongly buckled shapes are described by standard mechanics including fluctuation corrections. In this contribution, we estimate the optimal shape and the partition function of rigid filaments in both weak and strong buckling states. Fluctuations around the straight shape have been considered earlier [13]. We mainly consider filaments with freely rotating ends which applies, for example, to filaments attached to an isotropic bead in a laser trap. We also briefly consider filaments with their end orientations imposed, which applies to filaments glued on a rigid substrate (AFM tip) or to a zipping closure of a filament where the relative orientation for sticking is prescribed. The boundary conditions for the filament ends are demonstrated in Figure 1. Schiessel and Kulic argued that the DNA loop conformation on chromatin is mainly determined by energy considerations [23] and calculated the minimum energy spectrum for the size of extra loop using the Euler-Kirchhoff theory. Only planar configurations are sought in this study. The theory provided analytic results to some extent. However, for most boundary conditions, the ground-state conformation was obtained only by numerical minimization. Very recently the same group also added thermal fluctuations on top of the Euler solution [24] for a filament with imposed boundary angles.

[a] e-mail: lee@sejong.ac.kr

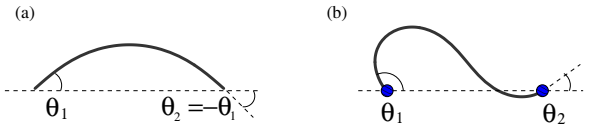

Fig. 1. A stiff chain under a compressive force. The vertical positions of both ends are fixed. The filament adopts its conformation in accord with boundary conditions: (a) the both ends can rotate freely and (b) the both boundary orientations are imposed.

Planar configurations are of special interest. Under most conditions, optimal configurations of filaments are planar. In some experiments the filaments are first deposited in a quasi 2-d flow chamber and the system is quasi 2-d by construction. Preliminary adsorption at liquid/liquid interface is also used to achieve fast kinetics of filament pairing or closure [25]. Also, real filaments often have non-isotropic section and there is a direction of easy bending [26] (cases with spontaneous twist, where the direction of easy bending is rotating, are more complicated). In the rest of this paper, we will mainly consider planar configurations.

A stiff molecule is modeled as a worm-like chain. Its configuration is described by the curve $\mathbf{r}(s)$, the position in space for a point of curvilinear coordinate s along the chain. The tangent unit vector is $\mathbf{u}(s) \equiv \partial\mathbf{r}(s)/\partial s$. Stiff molecules are characterized by the so-called "persistence length", l_p. The angular correlation $\langle \mathbf{u}(s) \cdot \mathbf{u}(s') \rangle$ decays exponentially with $|s - s'|$ over l_p along a long filament, due to thermal fluctuations. A filament of total length S will be called rigid if $S \ll l_p$. As we focus on the planar conformation, we leave out the twisting deformation [27,28] at this point. Later (Sect. 3.4), we will briefly discuss the influence of twisting on the filament shape when an out of plane fluctuation is allowed.

The Hamiltonian of the stiff chain associated with the bending energy can be written as

$$\frac{H}{k_B T} = \frac{l_p}{2} \int_0^S \mathrm{d}s \left(\frac{\mathrm{d}\mathbf{u}(s)}{\mathrm{d}s} \right)^2 . \tag{1}$$

This defines the partition function of the stiff chain:

$$Z = \int \mathcal{D}(\mathbf{u}(s)) e^{-H/k_B T} \tag{2}$$

and its free energy $F = -k_B T \ln Z$. Some general filament properties can be inferred from the structure of the Hamiltonian. For a given shape, the Hamiltonian H decreases with filament length as l_p/S. This can be seen by changing variables from s to s/S in the integral in equation (1). For very stiff chains much shorter than the persistence length for which $l_p/S \longrightarrow \infty$, the partition function is dominated by the shape that minimizes H. In these conditions, the unconstrained filament is completely straight. Under an external force, the Hamiltonian of the system consists of the contributions from the elastic (bending) energy and the potential energy.

$$\frac{H}{k_B T} = \frac{l_p}{2} \int_0^S \mathrm{d}s \frac{l_p}{2} \left[\left(\frac{\mathrm{d}\mathbf{u}(s)}{\mathrm{d}s} \right)^2 - \frac{\mathbf{f}}{k_B T} \cdot (\mathbf{r}(S) - \mathbf{r}(0)) \right] \tag{3}$$

For a prescribed shape, the Hamiltonian equation (3) under a force is also proportional to l_p/S as in the case of a free chain in equation (1), provided that the force is rescaled by the S-dependent $f_c \sim k_B T l_p / S^2$, which will be defined more rigorously later. This indicates that f/f_c, determines the optimal shape of the chain. The energy scale is l_p/S in thermal units and the ratio S/l_p measures the importance of fluctuations (some temperature dependence is formally hidden in l_p as $l_p = \kappa/k_B T$ with κ the bending modulus, the latter is used in Ref. [13]). Fluctuations around the optimal shape are negligible for comparatively short filament (vanishing S/l_p).

We first review the force-extension relation of the classical Euler-Lagrange solution (Sect. 2). Then in Section 3, we consider the influence of fluctuations and find that the extension is enhanced due to fluctuation at large buckling angles. We further consider cyclization triggered by compressive force. Buckling under various boundary conditions is discussed here.

2 The optimal shape of the compressed rigid filament: Euler elastica

First, we briefly recall the Euler-Kirchhoff theory, that describes the optimal shapes under constraints which serve as reference states for subsequent perturbative treatments of thermal fluctuations. The filament can be described by the contour parameter s and the angle $\theta(s)$ between its tangent $\mathbf{u}(s)$ and a reference direction $\hat{x}$. The integrations of $\sin\theta(s)$ and $\cos\theta(s)$ give y and x coordinates of the monomer, respectively. We choose the $\hat{x}$ direction along the end-to-end vector, so that $y(S) = y(0)$. In the Euler-Lagrange spirit, the Hamiltonian equation (3) corresponds to the action to be minimized. Under the given constraints, the action can be cast as

$$\mathcal{S} = \int \mathrm{d}s \left(k_B T \frac{l_p}{2} \left(\frac{\mathrm{d}\theta(s)}{\mathrm{d}s} \right)^2 - \mu \cos\theta(s) - \nu \sin\theta(s) \right). \tag{4}$$

The trajectory of the chain is described by the following "equation of motion":

$$k_B T l_p \frac{\mathrm{d}^2\theta(s)}{\mathrm{d}s^2} - \mu \sin\theta(s) + \nu \cos\theta(s) = 0, \tag{5}$$

where μ and ν are the x, y-components of the external force $\mathbf{f}$. At a fictitious cut, the torque exerted by the high-s side on the low-s side is $C(s) = k_B T l_p \frac{\mathrm{d}\theta(s)}{\mathrm{d}s}$. The Euler equation expresses the mechanical (possibly unstable) equilibrium under an applied force which states that torques on a small section of the filament are balanced.

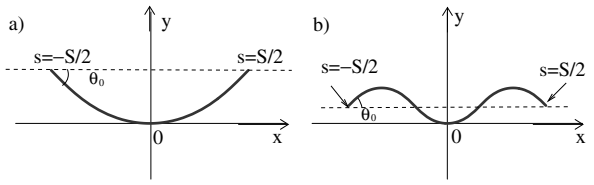

Fig. 2. (a) Coordinates of *Euler elastica* for symmetric conformations with clamped boundaries. (b) The excited state at given θ_0.

The Euler equation (Eq. (5)) yields the following first integral:

$$\frac{1}{2}k_BTl_p\left(\frac{\mathrm{d}\theta}{\mathrm{d}s}\right)^2+\mu\cos(\theta(s))+\nu\sin(\theta(s))=c. \qquad (6)$$

For the filament with freely orienting ends, there is no external torque exerted on the ends hence $C(0) = C(S) = 0$. The torque balance on the whole filament imposes that the force is along $\hat{x}$, *i.e.* $\mu = -\mathbf{f}$ and $\nu = 0$, as can also be seen by integrating equation (5) over θ along the filament. The Hamiltonian invariant in equation (6) then imposes $\cos(\theta(0)) = \cos(\theta(S))$. It is easy to see that the optimal shape under compression corresponds to $\theta(S) = -\theta_0$ where we set $\theta(0) = \theta_0$. Optimal configurations under compression are symmetric for freely orienting ends. The first integral equation (6) is simplified to

$$\frac{\mathrm{d}\theta}{2\mathrm{d}s/S}=\pi\sqrt{\frac{f}{f_c}}\sin(\theta_0/2)\left(1-\frac{\sin^2(\theta/2)}{\sin^2(\theta_0/2)}\right)^{1/2}, \qquad (7)$$

where $f_c = \pi^2 k_B T l_p/S^2$ will turn out to be the critical force for buckling (here thermal fluctuations are ignored) and f is the magnitude of the compression force. It is now natural to take the origin of the curvilinear coordinate s and of the spacial coordinates (x, y) at the middle of the filament (see Fig. 2). A successive integration of equation (7) leads to the optimal filament orientation $\theta(s)$:

$$\begin{aligned}\sin(\theta(s)/2)&=|\sin(\theta_0/2)|\,\mathrm{sn}\left(\frac{\pi s}{S}\sqrt{\frac{f}{f_c}},\sin^2(\theta_0/2)\right),\\ \cos(\theta(s)/2)&=\mathrm{dn}\left(\frac{\pi s}{S}\sqrt{\frac{f}{f_c}},\sin^2(\theta_0/2)\right),\end{aligned} \qquad (8)$$

and the filament shape

$$\begin{aligned}x(s)&=-s+\frac{2}{\pi}S\sqrt{\frac{f_c}{f}}\mathrm{E}\left(\frac{\pi s}{S}\sqrt{\frac{f}{f_c}},\sin^2(\theta_0/2)\right),\\ y(s)&=2\sin(\theta_0/2)\frac{S}{\pi}\sqrt{\frac{f_c}{f}}\\ &\quad\times\left(1-\mathrm{cn}\left(\frac{\pi s}{S}\sqrt{\frac{f}{f_c}},\sin^2(\theta_0/2)\right)\right),\end{aligned} \qquad (9)$$

where $\mathrm{sn}(u,m)$, $\mathrm{cn}(u,m)$ and $\mathrm{dn}(u,m)$ are Jacobian elliptic functions and $\mathrm{E}(u,m)$ is an incomplete Elliptic function [29]. From the first of equations (8), we see that $\frac{\pi}{2}\sqrt{\frac{f}{f_c}}$ is the quarter period given by the complete elliptic integral $\mathrm{K}(m)$. This determines the force-buckling angle relationship:

$$\sqrt{\frac{f}{f_c}}=\frac{2}{\pi}\mathrm{K}\big(\sin^2(\theta_0/2)\big). \qquad (10)$$

The above equations describe the buckled state. It is clear from equations (9) and (10) that the buckling angle θ_0 vanishes at the finite compression force f_c which was indeed announced as the critical force. The two branches and the standard square-root expansion close to the critical force $\theta_0 = \sqrt{8}\sqrt{\frac{f-f_c}{f_c}}$ are recalled in Figure 3. From

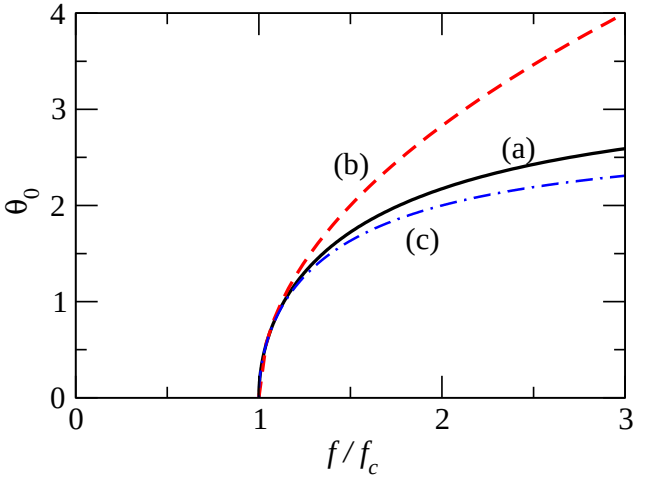

Fig. 3. Buckling angle θ_0 below/above the critical force f_c under the condition of free rotation at boundaries. (a) Euler-Lagrange solution given by equation (10), (b) asymptotic behavior close to the transition $\theta_0 = \sqrt{8\frac{f-f_c}{f_c}}$ (c) the mean values of the buckling angle in the first-mode approximation.

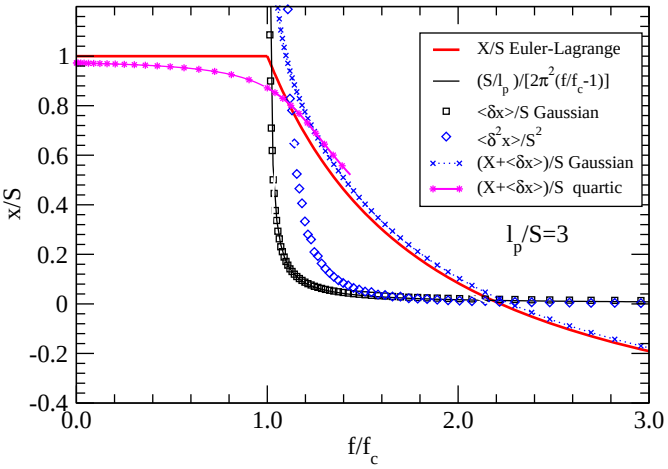

Fig. 4. Extension *vs.* force relations of a filament with $l_p/S = 3$. Bold line is from the ground-state description of the Euler-Lagrange equation. The correction to the ground state is evaluated when fluctuations are taken into account before and after the buckling transition in quadratic and quartic order of $\delta\theta$. The size of fluctuations $\langle\delta x\rangle$ and $\langle\delta^2 x\rangle$ are also indicated by symbols.

The above equations describe the buckled state. It is clear from equations (9) and (10) that the buckling angle θ_0 vanishes at the finite compression force f_c which was indeed announced as the critical force. The two branches and the standard square-root expansion close to the critical force $\theta_0 = \sqrt{8}\sqrt{\frac{f-f_c}{f_c}}$ are recalled in Figure 3. From

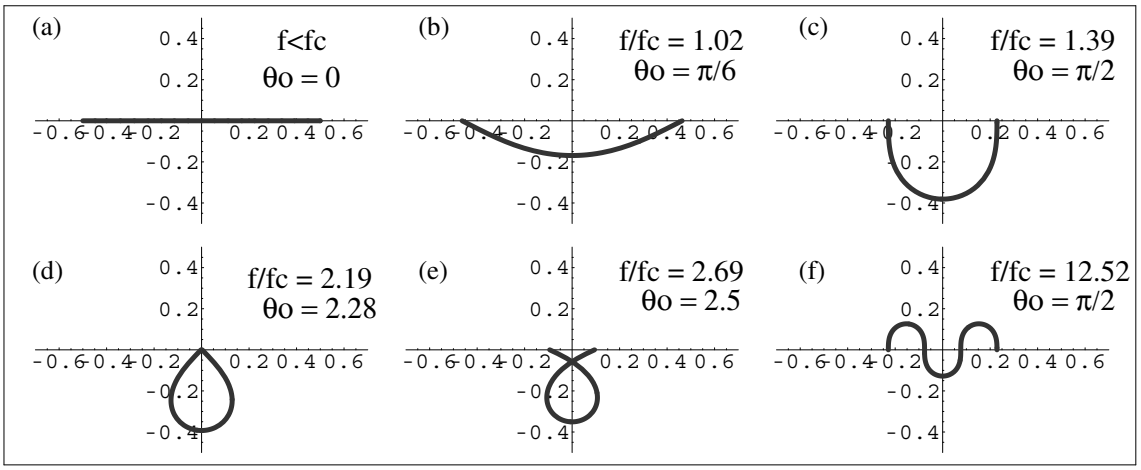

Fig. 5. Various conformations of a stiff chain below and above the bifurcation transition obtained from the Euler-Lagrange equation.

equations (9) the end-to-end extension of the filament is

$$X = S\left(-1 + 2\frac{\mathrm{E}\big(\sin^2(\theta_0/2)\big)}{\mathrm{K}\big(\sin^2(\theta_0/2)\big)}\right) \tag{11}$$

and later this will be corrected by fluctuations. Force extension laws are represented in Figure 4. The closed configuration corresponds to $f/f_c = 2.19$ and $\theta_0 = 2.28$. This shape is of special interest as it has the lowest bending energy among all possible closed filament shapes (up to corrections due to fluctuations). The angle between internal filament strands at contact is 1.42.

Equation (10) is not the only solution to equation (7) but the one with the lowest energy. There are also excited states representing local minima of the energy. These are given by $\sqrt{\frac{f}{f_c}} = p\frac{2}{\pi}\mathrm{K}(\sin^2(\theta_0/2))$ with p an odd integer. For a given θ_0, all optimal states (including the ground state $p = 1$) correspond to the same end-to-end extension (as can be also seen from $\mathrm{E}(p\mathrm{K}) = p\mathrm{E}(\mathrm{K})$). Comparing the bending energies, $U_b = f(X - S\cos(\theta_0))$, of the various states for the same separation X, $U_b(p) = p^2 U_b(1)$, the first excited state has a bending energy nine times that of the ground state. In microtubule networks [30], due to the presence of surrounding cytoskeletons, the observed buckling wavelength is also much smaller than the filament length. Figure 5 displays the shapes of the filament, so-called *Euler elastica*, for some typical buckled states. Figures 5(c) and (f) illustrate the ground state and first excited state for $\theta_0 = \pi/2$. The total energy $U_t = U_b + Xf$ can be expressed in terms of force and $m = \sin^2(\theta_0/2)$:

$$\frac{U_t(f,m)}{k_BT} = Sf\left(2m - 3 + \frac{4\mathrm{E}(m)}{\pi}\sqrt{\frac{f_c}{f}}\right). \tag{12}$$

3 Fluctuations

Next we will take into account fluctuations around the optimal shape $\theta_{EL}(s)$. To do so, we may expand the Hamiltonian around $\theta_{EL}(s)$, $\mathcal{H} = \mathcal{H}_{EL} + \mathcal{H}_{fl}$. Below we find it more convenient to choose the origin of s at a filament end. To Gaussian order the fluctuation Hamiltonian $\mathcal{H}_{fl}$ reads

$$\frac{\mathcal{H}_{fl}}{k_BT} = \int_0^S \mathrm{d}s\left[\frac{l_p}{2}\left(\frac{\mathrm{d}\delta\theta(s)}{\mathrm{d}s}\right)^2 + \frac{\mu}{2k_BT}\cos\theta_{EL}(s)\delta\theta(s)^2 + \frac{\nu}{2k_BT}\sin\theta_{EL}(s)\delta\theta(s)^2\right], \tag{13}$$

where $\delta\theta(s) = \theta(s) - \theta_{EL}(s)$ is the deviation from the Euler-Lagrange solution. The bending contribution can be transformed to $\left[\frac{l_p}{2}\delta\theta(s)\frac{\mathrm{d}\delta\theta(s)}{\mathrm{d}s}\right]_0^S - \frac{l_p}{2}\int_0^S \mathrm{d}s\delta\theta(s)\frac{\mathrm{d}^2\delta\theta(s)}{\mathrm{d}s^2}$ by integration by part. For both fixed boundary angle and freely rotating boundary angle, the bracket vanishes. Defining the operator $\hat{H} = -l_p\frac{\mathrm{d}^2}{\mathrm{d}s^2} + U(s)$ with $U(s) = \frac{\mu}{k_BT}\cos\theta_{EL}(s) + \frac{\nu}{k_BT}\sin\theta_{EL}(s)$, we arrive at $\frac{\mathcal{H}_{fl}}{k_BT} = \frac{1}{2}\langle\delta\theta|\hat{H}|\delta\theta\rangle$. The partition function associated with $\mathcal{H}_{fl}$ can be calculated from the spectrum of $\hat{H}$. In the standard situation, the expansion is carried out around a stable equilibrium and the spectrum is positive.

$$\mathcal{Z}_{fl} = \prod_n \sqrt{2\pi/\lambda_n}, \tag{14}$$

where λ_n's are the eigenvalues of $\hat{H}$. This product will turn out to be divergent due to short-wavelength modes. For real filaments, the finite thickness is a natural cut-off, as shorter modes cannot be treated in our description. In the remainder, we rather normalize $\mathcal{Z}_{fl}$ by its value in the absence of force, $\mathcal{Z}_{fl}^0$, to eliminate this divergence. Under a fixed compression force as considered here, there is an unstable mode, corresponding to a negative eigenvalue. The physical reason for this mode is clear: the compression equilibrium we are describing is unstable and an extra constraint is necessary to prevent, say, the global rotation towards the stable equilibrium where the applied force is pulling and the Euler-Lagrange shape is straight. This will be discussed in the following sections.

3.1 Fluctuation in unbuckled states

A slightly constrained filament under $f < f_c$ does not buckle and its optimal shape is straight ($\theta_{EL}(s) = 0$). Fluctuations do depend on the applied force: we expect a compression force to enhance fluctuations, much so if the buckling transition is approached. An extensional force *irons* the filament and the projected length ultimately matches S for a diverging force. Let us take the example of filaments with freely orienting ends (no localized torque is applied to the filament edges). The eigenmodes of $\hat{H}$ are $\psi_n(s) = \sqrt{\frac{2}{S}}\cos(\pi n s/S)$ for $n > 0$ and $\psi_0 = 1/\sqrt{S}$ with the spectrum $\lambda_n = n^2 f_c/k_BT - f/k_BT$. The mode $n = 0$ is unstable which corresponds to a global rotation of a straight filament. The stability is marginal for a vanishing force where the system is invariant under rotation. A given deviation from the straight shape is represented as $\delta\theta(s) = \sum_n A_n\psi_n(s)$. The global displacement $y(S)-y(0) = \int_0^S \delta\theta(s)\mathrm{d}s = A_0\sqrt{S}$ only depends on A_0, to lowest order in $\delta\theta$. It is hence enough to constrain the ends to be aligned on $\hat{x}$ to remove the rotation instability, without affecting the other modes. In practice one could use an anisotropic laser trap. It is easy to see how a harmonic y-potential can stabilize the $n = 0$ mode[1]. Assuming a strong reduction of this mode, for simplicity, we omit the corresponding factor in the infinite product:

$$\frac{\mathcal{Z}_{fl}}{\mathcal{Z}^0_{fl}} = \sqrt{\frac{\pi\sqrt{\frac{f}{f_c}}}{\sin\left(\pi\sqrt{\frac{f}{f_c}}\right)}}\,, \tag{15}$$

$$\mathcal{F}_{fl} - \mathcal{F}^0_{fl} = \frac{k_BT}{2}\log\frac{\sin\left(\pi\sqrt{\frac{f}{f_c}}\right)}{\pi\sqrt{\frac{f}{f_c}}}\,, \tag{16}$$

which characterizes the decrease of the free energy by the fluctuations. For weak compressive forces much weaker than the one causing the buckling transition $\mathcal{F}_{fl} - \mathcal{F}^0_{fl} \approx -\frac{k_BT\pi^2}{12}\frac{f}{f_c}$, this leads to the length stored in fluctuations at a vanishing force $\Delta L = \frac{S^2}{12l_p}$, which is small compared to S in the limit of rigid filament ($S/l_p \ll 1$). As expected, the free-energy reduction diverges at the buckling instability. The length stored in fluctuations,

$$\Delta L = \frac{\pi^2 k_BT}{4f_c}\left(\frac{\cot\left(\pi\sqrt{\frac{f}{f_c}}\right)}{\pi\sqrt{\frac{f}{f_c}}} - \frac{1}{\pi^2\frac{f}{f_c}}\right), \tag{17}$$

becomes unphysical (formally larger than S) for $(f_c - f)/f_c < S/(\pi^2 l_p)$ (it was argued that this criterion qualitatively locates the buckling transition under fluctuations [13]) and formally diverges at the transition as $\Delta L \simeq -\frac{k_BT}{2(f-f_c)}$ when calculated to quadratic order, this we further discuss below. Let us first notice that equation (16) remains true under an extensional force of the magnitude f, provided that "sin" is replaced by "sinh". In this way, one can calculate the length stored in fluctuations under extension and recover that it vanishes as $1/\sqrt{f}$ at high f, $\Delta L = \frac{S}{4}\sqrt{\frac{k_BT}{fl_p}}$ (if two equivalent bending directions are allowed (3-d) the length stored in fluctuations is doubled). The latter result, was obtained earlier [8] for the strong stretching regime of a long semi-flexible chain and has been proved very useful for DNA stretching experiments.

3.2 Buckling

Close to the buckling transition, the expansion of the Hamiltonian equation (13) in the A_n has to be carried out to higher orders. We expect the main physics to be captured by expanding to quartic order in the amplitude A_1 of the unstable mode and to quadratic order for others:

$$\begin{aligned}\frac{\mathcal{H}_{fl}}{k_{\mathbf{B}}T} &\approx \int_0^S \left\{-\frac{l_p}{2}\delta\theta\frac{\mathrm{d}^2\delta\theta}{\mathrm{d}s^2} - \frac{f}{2k_BT}(\delta\theta)^2 + \frac{f}{24k_BT}(\delta\theta)^4\right\}\mathrm{d}s \\ &= \frac{\lambda_1}{2}A_1^2 + \sum_{n=2}^{\infty}\frac{\lambda_n}{2}A_n^2 \\ &\quad + \frac{f/S}{24k_BT}\left\{\frac{3}{2}A_1^4 + 2A_1^3A_3 + \sum_{n=2}^{\infty}6A_1^2A_n^2\right\}. \end{aligned} \tag{18}$$

After having integrated out the amplitudes of the stable modes, we arrive at the reduced partition function $\mathcal{Z}_{fl}/\mathcal{Z}^0_{fl}$:

$$\begin{aligned}\frac{\mathcal{Z}_{fl}}{\mathcal{Z}^0_{fl}} &= \sqrt{\frac{f_c}{2\pi k_BT}}\int_{-\infty}^{+\infty}\mathrm{d}A_1\exp\left[\frac{-\tilde{H}_1}{k_BT}\right], \\ \tilde{H}_1 &= H_1 + \frac{1}{2}\log\frac{\sin\pi\sqrt{\frac{f}{f_c}\left(1-\frac{A_1^2}{2S}\right)}}{\pi\sqrt{\frac{f}{f_c}\left(1-\frac{A_1^2}{2S}\right)}\left(1-\frac{f}{f_c}\left(1-\frac{A_1^2}{2S}\right)\right)}, \end{aligned} \tag{19}$$

where H_1 collects terms in equation (18) depending on A_1 only: $H_1 = \frac{\pi^2 l_p}{S}(\frac{A_1^2}{2S}(1 - f/f_c) + \frac{1}{4}\frac{f}{f_c}(\frac{A_1^2}{2S})^2)$. No further approximation was made during the integration over the amplitude of the stable modes. The above expression equation (19) of $\tilde{H}_1$ makes sense, provided the argument of the logarithm is positive. For $A_1^2/(2S) < 1$, this requires $f < 4f_c$, for $A_1^2/(2S) > 1$ the expression still formally makes sense but "sin" is better rewritten as a "sinh", yielding: $\frac{1}{2}\log\frac{\sinh\pi\sqrt{\frac{f}{f_c}(\frac{A_1^2}{2S}-1)}}{\pi\sqrt{\frac{f}{f_c}(\frac{A_1^2}{2S}-1)}(1+\frac{f}{f_c}(\frac{A_1^2}{2S}-1))}$. It should however be noted that large $\frac{A_1^2}{2S}$ implies large fluctuation of the buckling angle. It means that the initial small buckling angle expansion becomes inaccurate. Assuming that the fluctuation of the buckling angle is smaller than one (which does apply

[1] Assume a harmonic y potential $V_y = \frac{1}{2}K_y(\delta y)^2$ acting on one end (bead) the other end being fixed in space and freely articulated. This contributes an extra energy $\frac{1}{2}K_yS(A_0)^2$ removing the instability provided $K_y > \frac{f}{S}$. The omited factor in equation (16) is $1/\sqrt{1 - f/(K_yS)} \approx 1$.

at least away from the buckling transition) we may expand the effective Hamiltonian $\tilde{H}_1$ to first order in $A_1^2/(2S)$:

$$\tilde{H}_1 = \ldots + H_1 + \left(\frac{3}{4} + \frac{1}{2(f/f_c - 1)} - \frac{\pi\sqrt{f/f_c}}{4}\cot\left[\pi\sqrt{f/f_c}\right]\right)\frac{A_1^2}{2S} + O\left(\left(\frac{A_1^2}{2S}\right)^2\right), \quad (20)$$

where $\ldots$ stands for the contribution independent of A_1 summing the stable modes in the Gaussian approximation. If we further expand the right-hand side of equation (20) for f/f_c close to unity,

$$\tilde{H}_1 = \ldots + H_1 + \frac{3}{8}\frac{A_1^2}{2S} + O\left(\left(\frac{A_1^2}{2S}\right)^2\right). \quad (21)$$

The latter expression is also obtained from a direct expansion early in the calculation, it amounts to replacing the powers in the amplitudes of stable modes in the Hamiltonian equation (18) by their thermal averages. In the following we use the expanded equation (21) which is accurate, provided the fluctuation of the buckling angle is smaller than unity:

$$Z_1 = \int_{-\infty}^{+\infty} \mathrm{d}A_1 \exp\left[-\frac{1}{2}\frac{(\tilde{f}_c - f)}{k_B T}A_1^2 - \Gamma_4 A_1^4\right]. \quad (22)$$

The integration over A_n other than A_1 renormalizes the critical force (second-order vertex) by corrections of order of S/l_p. A similar correction is obtained for the fourth-order vertex. In our calculation this however does not make Γ_4 negative and the transition would remain continuous. We find $\tilde{f}_c = f_c(1 + \frac{3}{8\pi^2}\frac{S}{l_p})$. Our calculation holds for buckling angles smaller than unity. It fails to precisely locate the critical force and to describe the very critical region if fluctuations of the buckling angle are of order unity [13]. Keeping this limitation in mind, we calculate the fluctuations of the buckling angle and the force extension curve from equation (22). Close to the transition ($f \sim \tilde{f}_c$), the fluctuations are large but finite, and dominated by the mode $n = 1$. Hence $\langle\theta_0^2\rangle = \frac{2}{S}\langle A_1^2\rangle$. From equation (22), at $f = \tilde{f}_c$,

$$\langle\theta_0^2\rangle_{\tilde{f}_c} = \frac{2}{\pi}\frac{\Gamma[3/4]}{\Gamma[5/4]}\sqrt{\frac{S}{l_p}}. \quad (23)$$

When numerical estimates of the Euler Gamma function $\Gamma[x]$ are inserted, the amplitude is close to 0.86. Formally these fluctuations remain weak, but get much larger than those in the states far from the transition where they are proportional to $\frac{S}{l_p}$. The partition function Z_1 equation (22) can be integrated both below and above $\tilde{f}_c$ as a function of $\epsilon = 2\frac{\tilde{f}_c - f}{\tilde{f}_c}\sqrt{\frac{\tilde{f}_c{}^2 S}{k_B T f}}$:

$$Z_1(\epsilon) = 2\left(\frac{k_B T S}{f}\right)^{1/4} \mathrm{g}_{-,+}(\epsilon),$$
$$\mathrm{g}_-(x) = \frac{1}{2}\sqrt{x}\mathrm{K}_{1/4}\left(x^2/8\right)\exp\left(x^2/8\right), \quad (24)$$
$$\mathrm{g}_+(x) = \frac{\pi}{2^{3/2}}\sqrt{-x}\left(\mathrm{I}_{1/4}\left(x^2/8\right) + \mathrm{I}_{-1/4}\left(x^2/8\right)\right) \times \exp\left(x^2/8\right),$$

where $\mathrm{g}_{-,+}$ expressed in terms of the modified Bessel functions $\mathrm{K}_\alpha[x]$ and $\mathrm{I}_\alpha[x]$ apply below and above the transition, respectively. Far below the transition where $\mathrm{g}_-(x) \sim \sqrt{\frac{\pi}{x}}$, we recover the result of the quadratic approximation up to the replacement of f_c with $\tilde{f}_c$ which is unimportant in this limit. At $\tilde{f}_c$, $\mathrm{g}_-(0) = \mathrm{g}_+(0) = \Gamma(1/4)/2$. The fluctuation of the buckling angle can be derived from the partition function. Its value $\langle\theta_0^2\rangle$ normalized by that at the transition $\langle\theta_0^2\rangle_c$ is shown in Figure 6. For convenience, only the first mode that dominates close to and above the transition is taken into account. In the same coordinates, the Euler-Lagrange solution $2A_1^2/S = 8(1 - \tilde{f}_c/f)$ in the first mode approximation together with its asymptotic behavior close to the transition (already given earlier) is represented. It can be seen that close to the transition, the buckling angle fluctuates widely over both branches of the bifurcation. For $\frac{f}{\tilde{f}_c} \gg 1$, the fluctuations approach the value of the Euler-Lagrange solution. This means that the filament is localized close to one of the branches and has only a small probability to be found with an intermediate buckling angle. In practice, the filament can only switch branches upon crossing a huge energy barrier and for a physical waiting time, it appears localized on one branch. Next we briefly discuss fluctuations around one branch for a buckled filament away from the transition.

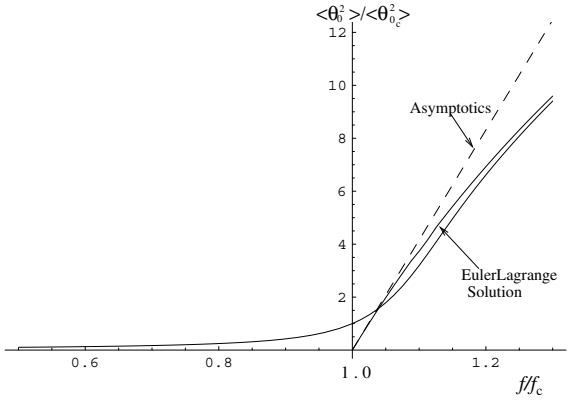

Fig. 6. Reduced buckling angle fluctuation $\frac{\langle\theta_0^2\rangle}{\langle\theta_0^2\rangle_c}$ (see text). The average buckling angle from the first mode approximation is shown together with its asymptotic close to the transition (dashed line). We choose $l_p/S = 20$.

3.3 Fluctuation around one branch, a buckled state

Not so far from the transition (for $\frac{f-\tilde{f}_c}{f_c} < 1$) the one-mode description only with the amplitude A_1 provides sufficient accuracy. The Euler-Lagrange branch is then approximated by $A_1^2 = \frac{f-\tilde{f}_c}{4k_BT\Gamma_4}$ and fluctuations around the upper branch A_1^+ are governed by the Hamiltonian $\delta H_1 = \frac{f-\tilde{f}_c}{k_BT}(\delta A_1)^2 + 4\Gamma_4 A_1^+(\delta A_1)^3 + \Gamma_4(\delta A_1)^4$, where the cubic term indicates a bias of the fluctuations towards the opposite branch. This free energy is double-well shaped with two equivalent minima located on the branches separated by a barrier of height $\frac{(f-\tilde{f}_c)^2 S}{fk_BT}$. As expected the barrier becomes relevant if the buckling angle markedly exceeds the fluctuation estimated in equation (23). Under these conditions, the fluctuations around one branch become relevant and $\langle(\delta\theta)^2\rangle = \frac{f_c S}{(f-\tilde{f}_c)\pi^2 l_p}$. The partition function $Z_1 \propto \sqrt{\frac{\pi}{f-\tilde{f}_c}}$ determines the variation of the projected length $\frac{\langle\delta x\rangle}{S} = \frac{f_c S}{2\pi^2(f-\tilde{f}_c)l_p}$ and its fluctuation $\langle(\delta x - \langle\delta x\rangle)^2\rangle = 2\langle\delta x\rangle^2$. The expression of $\langle\delta x\rangle$ obtained asymptotically below the transition (where $\langle\delta x\rangle = -\Delta L$) is identical, indicating that the force-extension curve rounded by fluctuations cuts the Euler-Lagrange curve in the transition region. Such a cut is provided by the quartic approximation discussed above. This seems to be a typical 2-d effect also found in simulations with fixed boundary angles in [24] based on bead-spring model.

In the general case we may seek for the spectrum of H for a finite buckling angle $\theta_0 \neq 0$. H has off-diagonal elements $\langle\psi_n|H|\psi_m\rangle$ when expressed in the base $\psi_n = \sqrt{2/S}\cos(\pi n s/S)$,

$$\begin{aligned}\langle\psi_m|H|\psi_n\rangle &= n^2\frac{f_c}{f} - \frac{2}{\pi}\sqrt{\frac{f_c}{f}}\int_{-\pi/2\sqrt{f/f_c}}^{\pi/2\sqrt{f/f_c}} \mathrm{d}u\psi_m(u) \\ &\quad\times\left(1 - 2\sin^2(\theta_0/2)\,\mathrm{sn}^2\left(u, \sin^2(\theta_0/2)\right)\right)\psi_n(u) \\ &= h_{mn}\frac{k_BT}{f} \qquad (25)\end{aligned}$$

with $u = \pi s/S\sqrt{f/f_c}$. Diagonalization gives eigenvalues λ_n of buckled states. The product of positive eigenvalues reduced by the zero force values λ_n/λ_n^0 converges when higher and higher modes n are included thereby increasing the size of the H matrix. In practice, it is usually sufficient to consider a 20×20 matrix. The force-extension relation corrected by fluctuation $(X + \langle\delta x\rangle)$ is shown in Figure 4.

With cyclization kinetics such as protein-mediated DNA looping [31,32] in mind, the closed (or nearly closed) conformations are of special interest [33]. From the Euler-Lagrange equation, we find that the stiff filament is closed at force $f_{cyc}/f_c = 2.18$ (see Fig. 5d) with a bending energy $E_b = 1.42\pi^2\frac{l_p}{S}k_BT$. The case when l_p/S remains moderate, say no more than 5, is of most practical interest, here again fluctuations become relevant. The shift $\langle\delta x\rangle = \delta F/\delta f$ in x away from closure is $0.055S^2/l_p$. As a consequence, closure ($\langle x\rangle = 0$) corresponds to a somewhat larger force shifted by $\delta f = k_BT\frac{\langle\delta x\rangle}{\sigma_x}$ with respect to the Euler-Lagrange estimate with $\sigma_x = -k_BT\mathrm{d}\langle x\rangle/\mathrm{d}f$ which is the fluctuation under force f_{cyc}. This shift in force corresponds to an additional shift in free energy $\delta F = k_BT\frac{(\langle\delta x\rangle)^2}{2\sigma_x}$. At this point we need to estimate σ_x, from the Euler-Lagrange solution $\sigma_x = 0.35\frac{S^3}{\pi^2 l_p}$ (the fluctuations add a correction $\propto S^4/l_p^2$), this is typically larger than the shift away from closure at f_c. The reduction of partition function when imposing $\langle x\rangle = 0$ as compared to the free state is $\exp\frac{-(E_b+\delta F)}{k_BT}$ with $\delta F/k_BT = -0.32 + 0.04S/l_p$. The (positive) correction arising from the shift $\langle\delta x\rangle$ is small for $l_p/S > 1$.

3.4 Symmetric fixed-angle boundary condition and a zipped state

So far, we have focused on the special case in which there is no torque exerted on the filament ends. The resulting conformations are naturally symmetric. In this section, we consider a symmetric conformation with the end orientations imposed. Quite often binding of two filament strands requires a special relative orientation [31,34,35]. Formally the boundary condition requires $\delta\theta(0) = \delta\theta(S) = 0$. When both angles are fixed to θ_0 (up to sign) to impose a symmetric configuration, there is a circular equilibrium state ($f = 0$) with $X = S\frac{\sin\theta_0}{\theta_0}$. Smaller extensions correspond to squeezing. When the pushing force is increased, a state is reached where imposing the chosen angle does not require any external torque. This state is described by equations (10, 11) for freely rotating boundary angle discussed above. At the force given by equation (10), the shape displays an inflexion point at the filament edges. For a higher force, the inflexion points move inwards (see Fig. 7(a)). The parameter m of the Jacobian Elliptic functions is linked to the angle θ_c at the inflexion point: $m = \sin^2(\theta_c/2)$. The angle at the inflexion point θ_c and the boundary angle θ_0 are linked by equation (8) at $s = \pm S/2$:

$$\cos(\theta_0/2) = \mathrm{dn}\left(\frac{\pi}{2}\sqrt{\frac{f}{f_c}}, \sin^2\left(\frac{\theta_c}{2}\right)\right). \qquad (26)$$

If the filament is free to twist out of the plane, it will release some constraint by building a loop if $\theta_0 < \pi/2$ and the angle then switches from θ_0 to $\pi - \theta_0$ (*i.e.* Figs. 7(a), (b)). When the constraint is increased, the first possible twisted shape has an inflexion point at the edges and hence corresponds to the parameter $m = \cos^2(\theta_0/2)$. If the initial force is further imposed, the end-to-end distance increases beyond the neutral point $X = S\frac{\sin\theta_0}{\pi-\theta_0}$ to reach a new equilibrium. This is illustrated in Figure 7(c) for $\theta_0 = \pi/6$. Any cost for twisting will suppress or delay the transition. We do not want to discuss twisting energy in detail here as it depends on boundary conditions imposed for the torsion angle ϕ. If angle ϕ is free (as could be assumed if the end is inserted into a hollow cylinder fixing θ but allowing for free rotation ϕ around the fibre axis), there is no penalty for twisting. If the end sections are constraint with a fixed orientation ϕ, twisting requires a high torsion

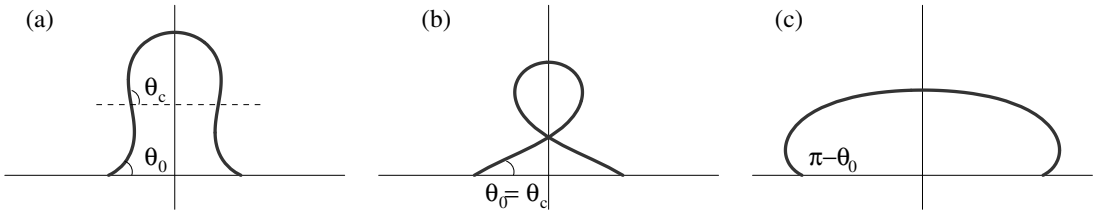

Fig. 7. Fixed-boundary-angle condition with $\theta_0 = \pi/6$ before and after twisting with $f/f_c = 2.217$ (a) At a large compressive force, the inflexion points exist at internal positions, $\theta_c > \theta_0$ and $m = \sin^2(\theta_c/2) = 0.93$. (b) Right after twisting, the inflexion points are at edges $\theta_c = \theta_0$. Here $m = \sin^2(\theta_0/2) = 0.57$ (c) The corresponding pulling force leads to the stretched conformation. The inflexion points exist on external points where contour shapes are extended. $\theta_c < \theta_0$, $m = 113.5$.

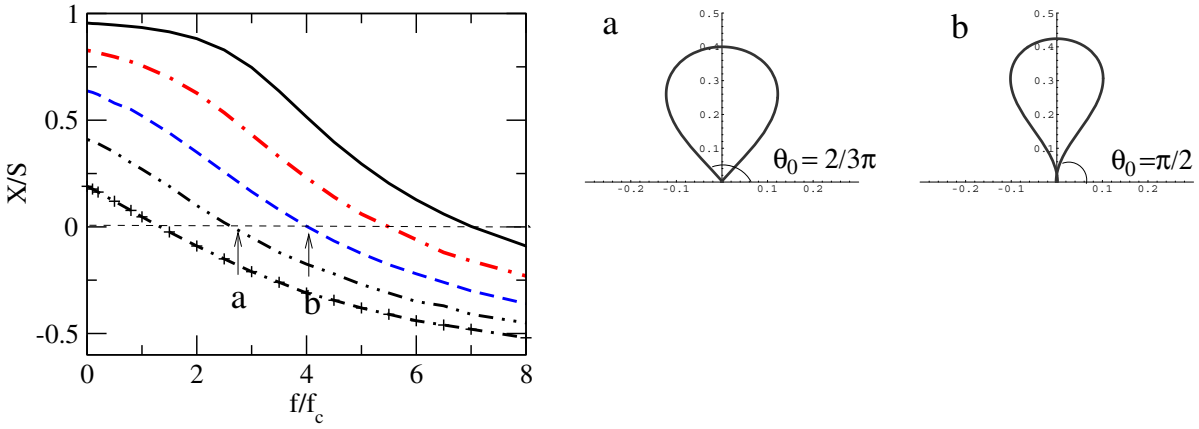

Fig. 8. Force-extension relations when the end orientation θ_0 is fixed as $\pi/6$, $\pi/3$, $\pi/2$, $2\pi/3$ and $5\pi/6$ from top to bottom. (Twisting is not allowed.) Closed shapes with preferred relative orientations are illustrated: (a) $\theta_0 = 2\pi/3$ with $m = 0.785$ and $f/f_c = 2.56$ and (b) $\theta_0 = \pi/2$ with $m = 0.731$ and $f/f_c = 4.01$, where the loop ends are antiparallel, leading to zipping.

Table 1. Bending energies and fluctuation of closed shapes with the imposed end orientations. The numbers in parenthesis ($\gamma = 2\theta_0 - \pi$) are the angles between the strands at closure.

$\theta_0(\gamma)$	f_x/f_c	$E_b/(\pi^2 l_p/S)(k_BT)$	m	δ F (k_BT)
$\frac{\pi}{2}(0)$	4.01	1.85	0.731	2.869
$\frac{2\pi}{3}(\frac{\pi}{3})$	2.56	1.44	0.785	2.806
2.28(1.42)	2.20	1.43	0.825	2.792
$\frac{3\pi}{4}(\frac{\pi}{2})$	2.0	1.43	0.858	2.788
$\frac{4\pi}{5}(\frac{3\pi}{5})$	1.6	1.47	0.958	2.780

energy $E_t = 2\pi^2 k_B T l_t/S$ with l_t a characteristic length which is typically larger then l_p (by about a factor 2 for DNA). Any soft constraint on ϕ like an elastic constraint modeled by a harmonic potential is in between. If the energy for twisting is not negligible, the twisted shape is prohibited or becomes stable at shorter end-to-end distances.

Together with equation (26), the force-extension relation at a given terminal orientation can be computed from equation (9). $X = \frac{2}{\pi} S \sqrt{\frac{f_c}{f}} \mathrm{E}(\frac{\pi}{2}\sqrt{\frac{f}{f_c}}, \sin^2(\theta_c/2)) - S$, where $m = \sin^2(\theta_c/2)$ replaces $\sin^2(\theta_0/2)$ in equation (26). In Figure 8, we demonstrate computed force-extension relations for specific end orientations. In particular, some closed shapes ($X = 0$) are illustrated for specific θ_0. We compute compressive force f_x acting on the loop termini and the corresponding bending energies in Table 1. The shift in extension due to fluctuation $\langle \delta x \rangle$ have positive values at all imposed angles. Thus, the required force to close a filament is larger than the classical estimation due to the fluctuations.

Table 1 demonstrates the bending energies and the fluctuations[2] of closed shapes for given imposed boundary angles θ_0. The numbers in parenthesis ($\gamma = 2\theta_0 - \pi$) represent the angles between the strands at closure. The bending energy minimum is found at $\theta_0 = 2.28$, $\gamma = 1.42$, nothing but the closure conformation with freely rotating ends (see Fig. 5(d)). On the other hand, the free-energy cost due to reduction of fluctuations (with respect to free

[2] When the boundary angles are fixed, the shape fluctuations are represented by linear combination of basis functions vanishing at the boundary $\delta\theta(S) = \delta\theta(0) = 0$. We thus expand $\delta\theta(s) = \sum_n B_n \xi_n$ with $\xi_n = \sqrt{2/S}\sin(\pi n s/S)$. ξ_n satisfies an equation similar to equation (25) where θ_0 in equation (25) is now replaced by θ_c given by equation (26):

$$\langle \xi_m | H | \xi_n \rangle = n^2 \frac{f_c}{f} - \frac{2}{\pi}\sqrt{\frac{f_c}{f}} \int_{-\pi/2\sqrt{f/f_c}}^{\pi/2\sqrt{f/f_c}} \mathrm{d}u \xi_m(u) \times \left(1 - 2\sin^2(\theta_c/2)\,\mathrm{sn}^2(u, \sin^2(\theta_c/2))\right)\xi_n(u) = h_{mn}\frac{k_BT}{f}.$$

filament) δF is largest when the strands are antiparallel at closure. δF is independent of the ratio l_p/S while the bending energy increase with l_p/S. Thus the favorable closure angle shifts (in practice slightly) from freely rotating case $\gamma = 1.42$ to larger closure angle γ as chain flexibility increases.

Zipped state. For rigid filaments small loops are disfavored and we may focus on the zipping cyclization. In our ideal (planar) filament picture, a natural requirement is that strands are antiparallel. Figure 8(b) corresponds to an interesting case where $\theta_0 = \pi/2$. All shapes for $f/f_c > 1.39$ ($m > 1/2$) display internal points with angle $\pi/2$. There is an internal strand satisfying all constraints and its shape provides a solution in the small force regime (after a proper size rescaling). A closed shape is obtained for $m = 0.731$ for a force of $f/f_c = 4.01$. The bending energy of the closed shape is $E_b = 1.85\pi^2 \frac{l_p}{S} k_B T$, where the prefactor is slightly higher than for the case of freely orienting filament edges. Note that bending the filament into a circle would correspond to higher bending energy with prefactor 2 instead of 1.85. If some zipping closure is induced by filament/filament binding with an energy gain δ_b per persistence length, the free energy of loop size s is $F = \frac{\delta_b}{2l_p} s + 1.85\pi^2 \frac{l_p}{s}$ in $k_B T$ units. By minimizing the free energy with respect to s, we find the terminal loop size $s_t = l_p \sqrt{3.7\pi^2/\delta_b}$, which can be quite smaller than l_p for a sufficiently large binding energy δ_b. Again fluctuation corrections are generally relevant.

Similarly as described in Section 3.3, we find the shift in δx away from the closed state to be $0.058 S^2/l_p$. This shift is about similar (slightly larger) to that under the freely rotating boundary condition.

3.5 Mixed boundary conditions

In this section, we discuss experimental situations where the boundary conditions are not symmetric.

Often, the filaments are subjected to mixed boundary conditions with one edge freely orienting and the other with a constrained orientation. The mixed boundary conditions are relevant to several experiments. In experiments on microtubules by Dogterom *et al.* [16,17] one end of the microtubule is blocked by a wall roughness and can rotate freely while at the other end the orientation β is adjusted to zero. Another example can be found in recent experiments of the deposition of CNT filaments in a two dimensional (2-d) chamber. CNTs are deposited on a striped surface [36] in a quasi 2-d flow chamber. As the filaments are rather rigid, they lie more or less straight on the adsorbing stripes. One edge typically fixes first. There are interesting stripe-edge effects shown in Figure 3 of reference [36]. If the adsorbing stripe width is smaller or comparable to the filament length, a filament typically leaves the stripe under an angle β and eventually binds back into the stripe. Prior to re-adsorption, the free end experiences no external torque and orients freely. By symmetry the preferred shape back into the stripe is symmetric. In order to minimize the bending energy, the turn involves the whole strand length available. However, as the adsorbed filament cannot reorient on the substrate but only slide at a fixed local orientation (as seems to be the case), the shape subsequently tightens under a longitudinal pulling force equal to the binding energy per unit length. The final orientation recollects the landing angle of the freely rotating end. The consideration of a mixed boundary condition allows us to discuss the statistical weight of less favorable shapes. We also found that the subsection of a DNA with multiple kinks can be described using mixed boundary condition [37]. Several proteins studied to date are shown to induce bends and kinks on DNA molecules upon binding [38–40]. During the measurement of elastic properties of DNA molecules, the whole chain is expected to adapt its conformation towards the optimal energy conformation by arranging each subchain between the neighboring kinks in skew-symmetric shape. The relative orientations of bond vectors at kinks are fixed by geometrical constraint set by chemistry.

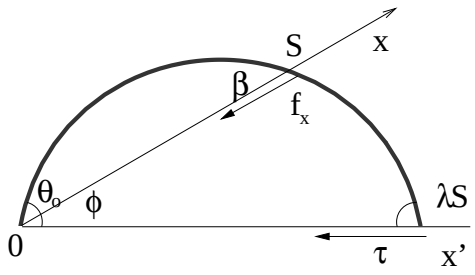

Fig. 9. The coordinates of *Euler elastica* in mixed boundary condition. The inflexion point is chosen as the origin. The actual shape is obtained by rotation of ϕ from the symmetric shape defined between two inflexion points. θ_0 is the angle at inflexion point and β the imposed angle at $s = S$.

If the boundary condition with freely rotating ends applies to both edges where the pulling force is exerted, the end-to-end vector is parallel to the external force (vanishing external torque condition). By the same reasoning, the internal inflexion points are also on the end-to-end line. Furthermore, if the sticking proteins are evenly spaced, inflexion points will be located in the middle of each subchain [41]. Under the mixed boundary condition, the resulting shapes are not usually symmetric. This also applies to the "equilibrium" shape where the force along the end-to-end vector vanishes. A relevant shape can be gained by a proper cut under an angle ϕ from a symmetric free orienting shape starting at one edge (see Fig. 9). Equations very similar to equations (8, 9) can be derived:

$$\frac{1}{2} k_B T l_p \left(\frac{\mathrm{d}\theta}{\mathrm{d}s} \right)^2 + \tau \cos(\theta(s) + \phi) = c. \qquad (27)$$

First, rather than using the two components of the force μ and ν, one may express the torque acting on the infinitesimal contour length ds with the magnitude of the force τ and its orientation ϕ as $\tau \sin(\theta + \phi)\mathrm{d}s$ (replacing the former $f \sin\theta \mathrm{d}s$). It is also more convenient to choose the origin for the arc length at the freely orienting edge.

$$\tan\phi = \Gamma(m) = \frac{2\sqrt{m}\sqrt{1-m}\,\mathrm{sd}\left(\pi\sqrt{\tau/f_c}, m\right)}{2\mathrm{E}\left(\pi\sqrt{\tau/f_c}, m\right) - 2m\,\mathrm{sn}\left(\pi\sqrt{\tau/f_c}, m\right)\mathrm{cd}\left(\pi\sqrt{\tau/f_c}, m\right) - \pi\sqrt{\tau/f_c}}\,. \tag{31}$$

This leads to the orientation

$$\begin{aligned}\sin((\theta+\phi)/2) &= \sqrt{m}\,\mathrm{cd}(u,m),\\ \cos((\theta+\phi)/2) &= \sqrt{1-m}\,\mathrm{nd}(u,m).\end{aligned} \tag{28}$$

The angles $\theta(s)$ can be expressed in terms of equations (28).

$$\begin{aligned}\sin\theta &= 2\left(\sin\left(\frac{\theta+\phi}{2}\right)\cos\left(\frac{\theta+\phi}{2}\right)\cos\phi\right.\\ &\quad\left.-\cos^2\left(\frac{\theta+\phi}{2}\right)\sin\phi+\frac{\sin\phi}{2}\right)\\ \cos\theta &= 2\cos^2\left(\frac{\theta+\phi}{2}\right)\cos\phi\\ &\quad+2\cos\left(\frac{\theta+\phi}{2}\right)\sin\left(\frac{\theta+\phi}{2}\right)\sin\phi-\cos\phi\end{aligned} \tag{29}$$

and the filament shape:

$$\begin{aligned}x(s) &= \frac{S}{\pi}\sqrt{\frac{f_c}{\tau}}\Big(-2\sin\phi\sqrt{m(1-m)}\,\mathrm{sd}(u,m)\\ &\quad+2\cos\phi\,(\mathrm{E}(u,m)-m\,\mathrm{sn}(u,m)\,\mathrm{cd}(u,m))\Big)-s\cos\phi,\\ y(s) &= \frac{S}{\pi}\sqrt{\frac{f_c}{\tau}}\Big(2\cos\phi\sqrt{m(1-m)}\,\mathrm{sd}(u,m)\\ &\quad-2\sin\phi\,(\mathrm{E}(u,m)-m\,\mathrm{sn}(u,m)\,\mathrm{cd}(u,m))\Big)+s\sin\phi,\end{aligned} \tag{30}$$

where $m = \sin^2((\theta_0+\phi)/2)$, $u = \frac{\pi s}{S}\sqrt{\frac{\tau}{f_c}}$, and $\mathrm{sn}(u,m)$, $\mathrm{cn}(u,m)$, $\mathrm{dn}(u,m)$ are Jacobian elliptic functions. The constraint $y(S) = 0$ links the angle ϕ and the parameter m of the Jacobian elliptic functions for the given force modulus τ.

See equation (31) *above*

The angle at the edge $s = S$ is imposed as β:

$$\begin{aligned}\cos\beta = \cos\phi\,\mathrm{f}(m) = \cos\phi\left(2(1-m)\,\mathrm{nd}^2\left(\pi\sqrt{\frac{\tau}{f_c}}, m\right)-1\right.\\ \left.+2\sqrt{m}\sqrt{1-m}\,\Gamma(m)\,\mathrm{nd}\left(\pi\sqrt{\frac{\tau}{f_c}}, m\right)\mathrm{cd}\left(\pi\sqrt{\frac{\tau}{f_c}}, m\right)\right).\end{aligned} \tag{32}$$

Following from the two constraints equations (31, 32), the parameter m of the Jacobian Elliptic functions satisfies

$$\cos^2\beta\left(1+\Gamma^2(m)\right) = \mathrm{f}^2(m). \tag{33}$$

All quantities of interest can now be calculated. For example, we get the free angle θ_0 from equations (29) as $\sin\theta_0 = \sin\phi(2m-1+2\sqrt{m}\sqrt{1-m}/\Gamma(m))$. The bending energy is now related to τ via $U_b = \tau(\cos\phi X - S\cos(\theta_0+\phi))$ and the total energy via $U_t = U_b + \tau\cos\phi X$.

When the imposed angle is non-zero, the neutral shape $f_x = 0$ is buckled, for our example ($\beta = \pi/6$), the free angle is $\theta_0 = 0.260$ and the end-to-end distance $0.973S$ ($\sqrt{2f_yS^2/(l_pK_BT)} = 1.79$). The magnitude of the free angle is always smaller than β for the neutral shape. Under compression the magnitude of the free angle increases and reaches that of the fixed angle. Here we recover a symmetric shape with an inflexion point at both edges and $f_y = 0$. Upon further compression the inflexion point moves from the fixed angle edge inward. The force is directed along the line joining the internal inflexion point and the free edge.

When $\beta = 0$, there is buckling transition at a larger compressive force than for the freely rotating edges case $\mu_c > f_c$. In order to find the critical compression force, we linearize equation (5): $l_p\frac{\mathrm{d}^2\theta(s)}{\mathrm{d}s^2} + \mu\theta(s) + \nu = 0$. The arclength position at s is $x(s) = \int(1-\frac{1}{2}\theta^2(s))\mathrm{d}s$ and $y(s) = \int\theta(s)\mathrm{d}s$. The Lagrangian multiplier μ is the compressive force in the x-direction. With the mixed boundary condition, we require $\partial\theta/\partial s|_0 = 0$ and $\theta(S) = \beta$. The solution to the differential equation has the following form: $\theta(s) = A\cos(s\sqrt{l_p/\mu}) + C$. Together with the constraint $y(s) = 0$, we obtain the buckling force μ_c as the smallest value of force μ satisfying the condition $\tan(x) = x$ with $x = \pi\sqrt{\mu/f_c}$.

$$\mu_c = 2.046 f_c = 20.19 k_B T l_p/S^2. \tag{34}$$

The critical compressive force μ_c under mixed boundary condition is about twice as large as f_c. This result agrees with the critical buckling force observed by Janson and Dogterom [17].

In Figure 10, we represent the end-to-end distance ($X = x(S)$) as a function of the longitudinal force $\tau\cos\phi$ for two values of the imposed angle: $\beta = 0$, $\beta = \pi/6$. One of ends can rotate freely in order to minimize the bending energy. Two types of force-extension measurement can be considered: i) a compressive force is given and ii) the total extension is controlled. With a vanishing force f_x, the filaments are at extension $X_0 = 0.973S$ for $\beta = \pi/6$ and at $X_0 = S$ for $\beta = 0$. For $\beta = 0$, the filament buckles at μ_c. As the compressive force increases, the orientation of the freely rotating end θ_0 increases with the tilted angle ϕ. For $\phi \neq 0$, the end with fixed orientation β experiences a net torque which should be balanced with the vertical component of the external force f_y. The free end of the chain escapes from the clamping edge unless there is force holding the end. The filament shapes are stable as long as the extension is a decreasing function of f_x. For a large tilted angle ϕ (beyond B, G), the buckled shapes become unstable. Under the constant force, the filament undergoes transition to the solutions in different branches. The transition is indicated as arrows in vertical

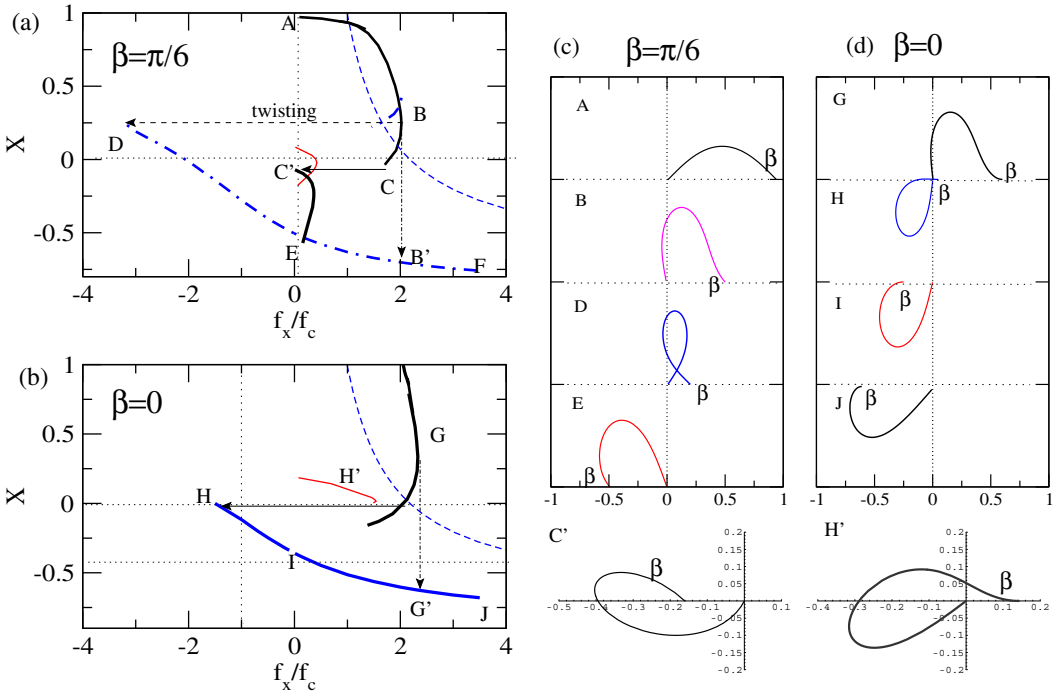

Fig. 10. Force-extension relations of a filament under mixed boundary condition. One chain end at origin ($X = 0$) can rotate freely (clamped) and the other end is imposed to start with an angle $\beta = \pi/6$ (top panel, a) and $\beta = 0$ (bottom panel, b). The force-extension curves of freely rotating ends are shown as dashed lines for comparison. Typical filament shapes at the marked positions are shown in (c) and (d). The thin solid lines represent a path with higher energy conformations. The dot-dashed line is obtained when twisting is allowed. The fixed angle β is indicated for each shape in panel (c) and (d).

direction (B $\rightarrow$ B′ and G $\rightarrow$ G′). Increase of f_x straightens the filament further. However, inflexion point can no longer exist at boundary beyond F, J.

During the force measurement under *controlled extension*, the force-extension path may depend on the constraint whether the filament is forbidden to twist. If one end is imposed to start with an angle $\beta = \pi/6$, the force-extension curve follows the solid line connecting (A, B) at large extensions. A transition to lower energy conformation occurs ($\theta_0 \rightarrow \pi - \theta_0$) if twisting is allowed. In Figure 10(a), such a transition under a given extension is indicated by the dashed horizontal arrows. After the transition, the necessary force to keep the filament at the given position switches the sign. The negative value of f_x indicates that the force is now "pulling" the end. The extension goes through the origin with increasing force following the lower curve (D $\rightarrow$ E $\rightarrow$ F). If twisting is not allowed, the path remains on the line connecting (A, B, C) until the hairpin-like conformation is formed. Then the path jumps from C to C′ where the conformation switches via rotation with respect to the inflexion point.

For $\beta = 0$, the filament remains on the solid line (G) until the extension vanishes. Then lower energy configurations are found at lower curve connecting (H, I, J). The transition to H (indicated by the arrow in Fig. 10(b)) is expected at $X = 0$ via rotation around the inflection point (without twisting). On further squeezing, the path remains on the thick solid line (H, I, J). The thin solid line represents conformations at intermediate extensions such as displayed in panel (d) as H′. These are energetically less favorable and their contribution to the equilibrium elastic response is expected to be negligible.

3.6 Asymmetric fixed-angle boundary conditions

It is worthwhile to briefly discuss the case when the angle is imposed at both edges at θ_1 and θ_2. The main difference with the mixed boundary is that the shift in the argument of Jacobian Elliptic function c is not a quarter period. It is to be determined from the known imposed angle θ_1 and θ_2,

$$\cos\left(\frac{\theta+\phi}{2}\right) = \mathrm{dn}(u+c,m), \tag{35}$$

$$\sin\left(\frac{\theta+\phi}{2}\right) = \sqrt{m}\,\mathrm{sn}(u+c,m), \tag{36}$$

with $u = s\pi/S\sqrt{\tau/f_c}$. After integration, we get

$$\begin{aligned} x &= \left(2\frac{S}{\pi}\sqrt{\frac{f_c}{\tau}}\big(\mathrm{E}(u+c,m)-\mathrm{E}(c,m)\big) - s\right) \\ &\times \cos\phi - 2\sqrt{m}\sin\phi\frac{S}{\pi}\sqrt{\frac{f_c}{\tau}}\left(\mathrm{cn}(u+c,m)-\mathrm{cn}(c,m)\right), \\ y &= -2\sqrt{m}\cos\phi\frac{S}{\pi}\sqrt{\frac{f_c}{\tau}}\left(\mathrm{cn}(u+c,m)-\mathrm{cn}(c,m)\right) \\ &+ \sin\phi\left(s - 2\frac{S}{\pi}\sqrt{\frac{f_c}{\tau}}\big(\mathrm{E}(u+c,m)-\mathrm{E}(c,m)\big)\right). \end{aligned} \tag{37}$$

The expression for a tilt angle ϕ can be represented in terms of τ, m and c from the constraint $y(S) = 0$.

$$\tan\phi = \Gamma_a(u+c,m) = \frac{2\sqrt{m}\sqrt{\frac{f_c}{\tau}}\frac{S}{\pi}(\mathrm{cn}(u+c,m)-\mathrm{cn}(c,m))}{s-2\sqrt{\frac{f_c}{\tau}}\frac{S}{\pi}\big(\mathrm{E}(u+c,m)-\mathrm{E}(u,m)\big)}. \quad (38)$$

By inserting equations (36) to equation (29), similarly to equation (32), we construct $f_a(u+c,m) = 2\,\mathrm{dn}^2(u+c,m)+2\sqrt{m}\,\mathrm{dn}(u+c,m)\,\mathrm{sn}(u+c,m)\Gamma_a(u+c,m) - 1$. At the boundaries $s = 0$ and S,

$$\cos^2\theta_1\big(1+\Gamma^2(c,m)\big) = f_a^2(c,m), \quad (39)$$

$$\cos^2\theta_2(1+\Gamma^2(\pi\sqrt{\tau/f_c}+c,m)) = f_a^2(\pi\sqrt{\tau/f_c}+c,m). \quad (40)$$

The unknown variables m, c and ϕ can be obtained from equations (38–40).

4 Conclusion

Unlike usual flexible polymers that coil under thermal noise, rigid filaments do by definition share many properties of macroscopic thin rods in a first approximation. On the other hand, only in extreme cases like microtubules or multiwall carbon nanotubes are shape fluctuations completely negligible for standard filament length. We tried to adapt the description of optimal rod shapes under compression to thin long rigid filaments. These are described by a persistence length l_p, over which the orientation correlations decay, markedly larger than the filament length S.

Several boundary conditions are considered. Two seem most relevant: the free-orienting-end case and the mixed boundary case where the orientation is fixed at one end. The former applies to filaments manipulated by optical or magnetic tweezers and the latter to many experiments where one end orientation is tuned. Deposition of filaments also sometimes falls in this category when the first adsorbed section (end) cannot change the orientation anymore. Fluctuations also control cyclization or zipping reactions of filaments, or some aspects of their deposition on striped surfaces as discussed above.

As also shown earlier [13] a free filament stores a fraction of its length, proportional to S/l_p in fluctuations. Under a compressive force, as considered here, the stored length increases and saturates at the buckling transition. In the strongly buckled states, fluctuations around the (one of the two) more favorable shape(s) are again weaker and essentially $\propto S/l_p$. We estimated fluctuation corrections to the force-extension curves. In two dimensions as considered here, the end-to-end distance under a given force is decreased by fluctuations in the unbuckled state and increased in the buckled state. The force-extension curve rounded by fluctuations hence crosses the Euler curve in the transition region. This crossing is at least qualitatively described by a calculation to quartic order. As a consequence the force needed to impose average closing ($\langle x\rangle = 0$) is larger than anticipated from *Euler elastica*. As shown explicitly in [24] for fixed boundary angles (also by simulation), if weak uncoupled in-plane and out-of-plane fluctuations are allowed (3-d), the end-to-end distance is decreased by fluctuations also in the buckled state. The, somewhat surprising, increase of the end-to-end distance in buckled state hence seems to be a peculiarity of 2-d filaments. The energy barrier against closing with free or prescribed angle is increasing with stiffness as $\propto l_p/S^2$ in thermal units, fluctuation corrections are estimated to be of order unity and become important for moderately rigid filaments. Similar conclusions hold for zipping. In the case of fixed boundary angles we showed that for $0 < \theta_0 < \pi/2$ a looped conformation may form under compression by twisting this is favoured by loose boundary conditions for the torsion angle and/or weak torsion modulus.

This work is supported by the Korea Science and Engineering Foundation (KOSEF) grant (R01-2007-000-10854-0) (N.-K.L.). S.-C.H. acknowledges the financial support from the Korea Research Foundation (KRF) funded by the Korean government through grant (MOEHRD, KRF-2006-C00132) and Korea Science and Engineering Foundation (KOSEF) grant (R01-2007-000-11674-0).

References

1. F. Gittes, E. Meyhofer, S. Baek, J. Howard, J. Cell Biol. **120**, 923 (1993).
2. M.G. Ancona, S.E. Kooi, W. Kruppa, A.W. Snow, E.E. Foos, L.J. Whitman, D. Park, L. Shirey, Nanolett. **3**, 135 (2003).
3. S. Iijima, Nature **354**, 56 (1991).
4. S.B. Smith, L. Finzi, C. Bustamante, Science **258**, 1122 (1992).
5. M. Rief, F. Oesterhelt, B. Heymann, H.E. Gaub, Science **275**, 1295 (1997).
6. J. Liphardt, B. Onoa, S.B. Smith, I. Tinoco, C. Bustamante, Science **292**, 733 (2001).
7. M.S.Z. Kellermayer, S.B. Smith, H.L. Granzier, C. Bustamante, Science **271**, 1112 (1997).
8. J.F. Marko, E.D. Siggia, Macromolecules **28**, 8759 (1995).
9. U. Gerland, R. Bundschuh, T. Hwa, Biophys. J. **84**, 2831 (2003).
10. N.-K. Lee, D. Thirumalai, Biophys. J. **86**, 2641 (2004).
11. E. Jarkova, N.-K. Lee, S. Obukhov, Macromolecules **38**, 2469 (2005).
12. T.R. Strick, J.F. Allemand, D. Bensimon, V. Croquette, Biophys. J. **74**, 2016 (1998).
13. Theo Odijk, J. Chem. Phys. **108**, 6923 (1998).
14. J. Berro, A. Michelot, L. Blanchoin, D.R. Kovar, J.-L. Martiel, Biophys. J. **92**, 2546 (2007).
15. Y. Zhao, L. An, J. Fang, Nanolett. **7**, 1360 (2007).
16. J.W. Kerssemakers, M.E. Janson, A. van der Horst, M. Dogterom, Appl. Phys. Lett. **83**, 4441 (2003).
17. M.E. Janson, M. Dogterom, Phys. Rev. Lett. **92**, 248101 (2004).
18. Y. Komarova, I.A. Vorobjev, G. Borisy, J. Cell Sci. **115**, 3528 (2002).

19. P. Ranjith, P.B.S. Kumar, Phys. Rev. Lett. **89**, 018302 (2002).
20. F.C. MacKintosh, J. Käs, P.A. Jammey, Phys. Rev. Lett. **75**, 4425 (1995).
21. Klaus Kroy, Erwin Frey, Phys. Rev. Lett. **76**, 306 (1996).
22. Claus Heussinger, Mark Bathe, Erwin Frey, Phys. Rev. Lett. **99**, 048101 (2007).
23. I.M. Kulic, H. Schiessel, Biophys. J. **84**, 3197 (2003).
24. Marc Emanuel, Hervé Mohrbach, Mehmet Sayar, Helmut Schiessel, I.M. Kulic, preprint cond-mat arXiv:011913.
25. A. Goldar, J.-L. Sikorav, Eur. Phys. J. E **14**, 211 (2004).
26. A. Nyrkova, A.N. Semenov, J.F. Joanny, A.R. Khokhlov, J. Phys. II **6**, 1411 (1996).
27. S. Neukrich, Phys. Rev. Lett. **93**, 198107 (2004).
28. A.V. Vologodskii, N.R. Cozzarelli, Annu. Rev. Biophys. Biomol. Struct. **23**, 609 (1994).
29. L.D. Landau, E.M. Lifshitz, *Theory of Elasticity* (Pergamon, New York, 1986).
30. C.P. Brangwynne, F.C. MacKintosh, S. Kumar *et al.*, J. Cell Biol. **173**, 733 (2006).
31. Y. Zhang, A.E. McEwen, D.M. Crothers, S.D. Levene, Biophys. J. **90**, 1903 (2006).
32. S. Jun, J. Bechhoefer, B. Ha, Europhys. Lett. **64**, 420 (2003).
33. M. Sano, A. Kamino, J. Okamura, S. Shinkai, Science **293**, 1299 (2001).
34. J.D. Kahn, D.M. Crothers, Proc. Natl. Acad. Sci. U.S.A. **89**, 6343 (1992).
35. Q. Du, C. Smith, N. Shiffeldrim, M. Vologodskaia, A. Vologodskii, Proc. Natl. Acad. Sci. U.S.A. **102**, 5397 (2005).
36. J. Im, L. Huang, J. Kang, M. Lee, S. Rao, N.-K. Lee, S. Hong, J. Chem. Phys. **124**, 224707 (2006).
37. P.M. Pil, S.J. Lippard, Science **256**, 234 (1992).
38. S. Ferrari, V.R. Harley, A. Pontiggia, P.N. Goodfellow, R. Lovell-Badge, M.E. Bianchi, Embo J. **11**, 4497 (1992).
39. Y. Tanaka, O. Nureki, H. Kurumizaka *et al.*, Embo J. **23**, 6612 (2001).
40. S.V. Kuznetsov, S. Sugimura, P. Vivas, D.M. Crothers, A. Ansari, Proc. Natl. Acad. Sci. U.S.A. **103**, 18515 (2006).
41. N.-K. Lee, S.-C. Hong, S. Obukhov, A. Johner, preprint.